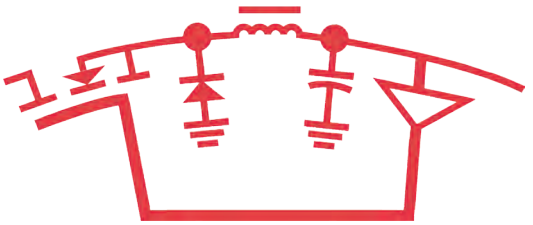

Power Supply Design Seminar

Power-Conversion Techniques for Complying with Automotive Emissions Requirements

Reproduced from
2020 Texas Instruments Power Supply Design Seminar
SEM2400
Topic 1
TI Literature Number: SLUP389

Power Supply Design Seminar resources
are available at:
www.ti.com/psds

Texas Instruments

Power-Conversion Techniques for Complying with Automotive Emissions Requirements

Josh Mandelcorn and Pradeep Shenoy

ABSTRACT

Comité International Spécial des Perturbations Radioélectriques (CISPR) 25 is the typical starting point for evaluating conducted and radiated emissions in automotive systems [1]. This topic addresses the unique challenges of designing power converters to pass automotive EMC requirements based on CISPR 25 requirements, including background information on the CISPR 25 standard and test setups. We explain common noise sources in power converters and various techniques to reduce conducted and radiated emissions, including input filter design, frequency selection, mode selection, snubber design, shielding and layout. Measured results from a 13.5 V input to a 3.3 V, 5 A output converter case study demonstrate the relative effectiveness of electromagnetic interference (EMI) mitigation techniques and the path to passing CISPR 25 Class 5 conducted emissions.

I. INTRODUCTION

Consider a scenario where you are listening to the radio in a car. There is noise right in the frequency band of the radio station you are trying to listen to. Unfortunately, the power converters supplying the adaptive cruise control system are generating unwanted emissions (noise) as shown in Figure 1. You cannot hear clearly due to the interference. If the radio station is only playing music, this scenario will probably just be annoying. If you are trying to get important weather or road conditions information, this scenario could be quite disruptive.

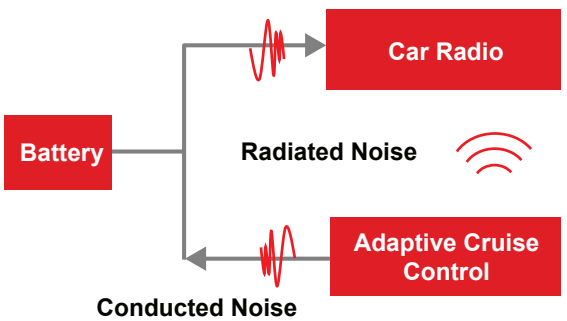

Figure 1 – Conducted and radiated noise in vehicle systems can cause unwanted interference.

What if the hypothetical scenario above was reversed? What if the radio system generated noise that interfered with the adaptive cruise control system? It is possible that the interference could cause the cruise control to malfunction which could be deadly. For these reasons, there are strict limits on emissions in vehicles. Car manufacturers want to ensure that electromagnetic interference (EMI) does not cause any problems.

This paper examines several techniques to help comply with automotive emissions requirements. Power converters are often the source of electromagnetic emissions, and it is important to ensure power supply systems achieve the appropriate level of electromagnetic compatibility (EMC). CISPR 25 is a commonly used standard that defines test methods and limits to conducted and radiated emissions for electronic components in vehicles.

This paper introduces the sources and types of emissions typically seen in power supplies. Various methods to mitigate emissions are presented including filtering, component selection, printed circuit board (PCB) layout and circuit techniques. The goal is to enable the reader to design power converters that pass EMI test requirements. A case study is included to experimentally demonstrate the relative effectiveness of the mitigation techniques discussed in an example application. The example converter is designed for a nominal 13.5 V input and 3.3 V, 5 A output and achieves CISPR 25 Class 5 limit compliance for conducted emissions.

It is worth noting several of the unique challenges facing automotive converter design. Power converters connected to typical 12 V lead acid batteries in vehicles must be designed to handle wide input voltage variations as shown in Figure 2. The input voltage can dip significantly (to less than 4 V) when the internal combustion engine is started and can rise as high as 40 V during load dump or battery disconnect scenarios. This requires higher voltage rated switching circuits.

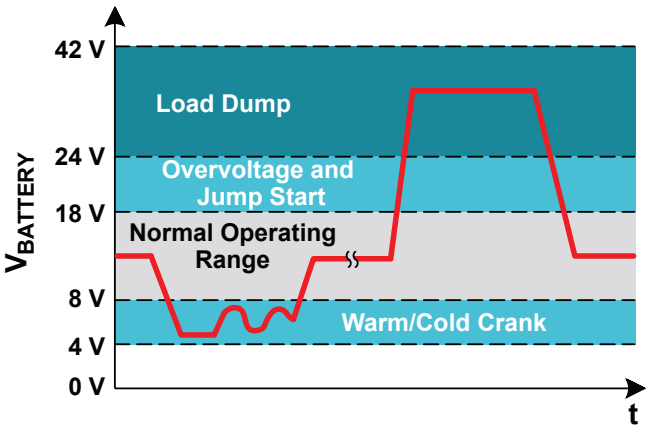

Figure 2 – Off-battery power converters are designed to handle the wide voltage range at their input.

Automotive environments present challenges for making low EMI power solutions. Vehicles are known for considerable vibration and mechanical stress. Certain construction methods used in other applications to reduce parasitic inductance are not able to withstand the stresses of the automotive environment. Components with leaded packages are preferred at times for low-cost manufacturing and inspection but tend to increase parasitic inductance. Sometimes two series-connected ceramic capacitors are placed on a PCB at a 90 degree angle to provide redundancy in case one of them fails short. This technique also increases parasitic inductance. The operating temperature range is also quite wide, often from -40°C to 125°C, and cooling fans may not be an option. Despite these challenges, design of low EMI power converters is achievable.

II. Background on Emission Sources

To gain a basic understanding of the sources of electromagnetic emissions in power converters, consider the system depicted in Figure 3. This diagram represents the conventional power delivery system for an electronic control unit (ECU) powered by a lead acid battery. (Power can also come from the alternator which is not shown.) A wiring harness connects the battery to the ECU and switching converters (like the buck converter shown in the diagram) to provide regulated supply voltages to the ECU loads, which could be a second stage converter, digital processor, memory or some other system on chip (SoC).

Figure 4 depicts several important time-domain waveforms of a switching power converter. The switch-node voltage, shown in Figure 4(a), alternates between 0 V and the input voltage (typically around 13.5 V). The rise and fall times of the switch-node voltage are fairly short (several nanoseconds) resulting in high dv/dt edges during switching transitions. These fast edge rates combined with capacitive and magnetic coupling are one cause of emissions in switching converters. Similarly, as shown in Figure 4(b), the current through the high-side switch in the buck converter pulses every switching cycle. The short rise and

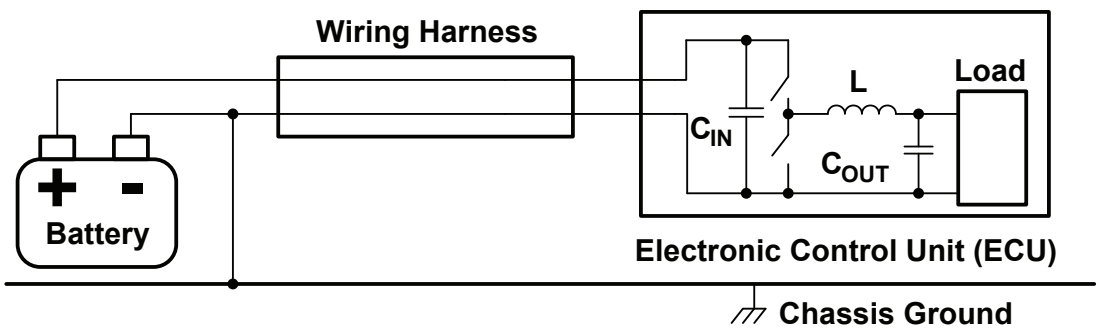

Figure 3 – Simplified power delivery diagram for an automotive electronic control unit.

fall time of the switch current results in high di/dt edges of the current waveform, which are another source of emissions. The switch current pulses cause ripple in the input voltage waveform shown in Figure 4(c). Even with only 50 mV of voltage ripple, the magnitude of the fundamental component is over 90 dBµV, which is beyond the typical limits for conducted emissions.

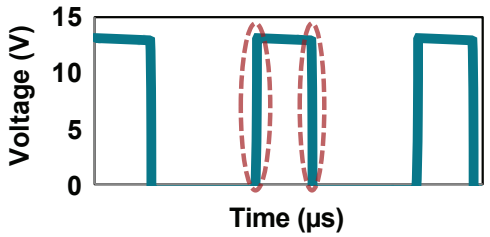

(a)

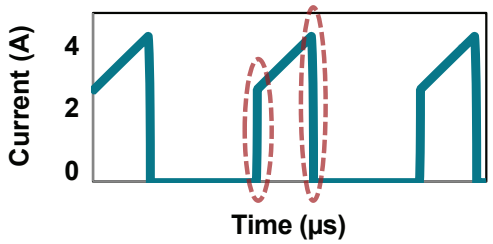

(b)

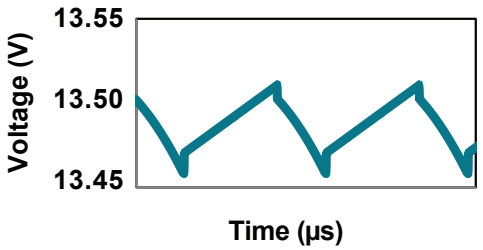

(c)

Figure 4 – Time domain waveforms of (a) switch-node voltage, (b) high-side switch current and (c) input capacitor voltage in an example buck converter.

Decomposing a time domain signal into its frequency components helps to understand where noise emissions may be coming from. The Fourier transform is used to convert the time-domain waveforms to the frequency domain. Recall that any periodic signal can be represented as the sum of sinusoidal waveforms as expressed in Equation (1).

$$f(t) = \sum_{n=0}^{\infty} c_n \cos(n\omega t + \theta_n) \quad (1)$$

An example plot showing the magnitude of each frequency component of a time-domain waveform is shown in Figure 5. The frequency component with the largest amplitude occurs at the switching frequency of the power converter (the fundamental frequency). The magnitude peaks decrease as frequency increases with the higher order harmonics.

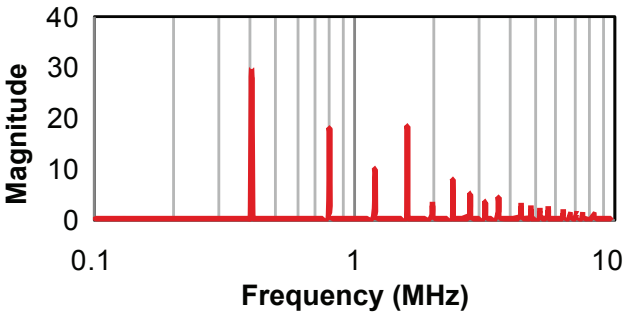

Figure 5 – The frequency content of a time domain signal is found by applying the Fourier transform.

III. Automotive EMI Standards

A common emissions standard in automotive is CISPR 25. While vehicle manufacturers often will have their own modified set of emissions limits, CISPR 25 is widely used for evaluating automotive equipment. The standard defines not only the emissions limits but also the test setup and procedures.

Figure 6 shows the peak limits for conducted and radiated emissions that meet CISPR 25 Class 5. There are lower class levels that have less stringent EMI limits [1-3]. The conducted limits (shown in blue) span from 150 kHz to 108 MHz and are measured in dBµV. The radiated limits (shown in red) apply from 150 kHz to 2.5 GHz and are measured in dBµV/m. There are also average and quasi-peak limits for conducted and radiated emissions not shown in Figure 6. The goal for compliance is to ensure that the frequency content of the equipment under test does not exceed (is not greater than) the specified limits.

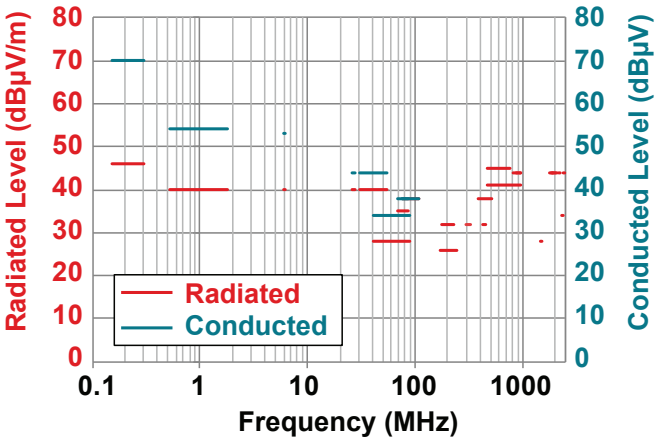

Figure 6 – Radiated and conducted peak emissions limits for CISPR 25 Class 5.

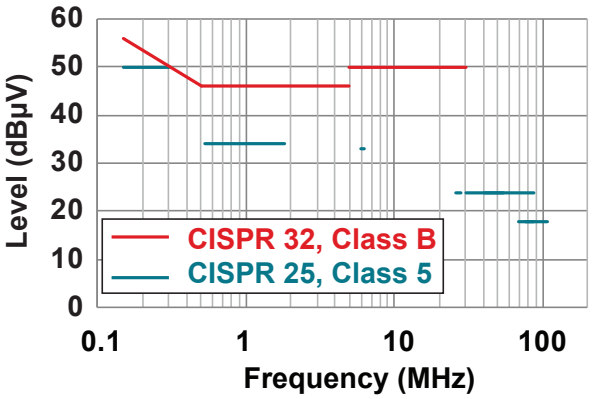

Figure 7 – Conducted average limits comparison CISPR 32, Class B vs. CISPR 25, Class 5.

It is worth noting that there are gaps in the limit lines. This indicates that there is no limit in frequencies between limit lines. Power converter designers often select the switching frequency to occur at a "gap" in the limits. (Some car manufacturers extend the limits to cover the frequency gaps.) A particular frequency band that is avoided is the AM band between about 500 kHz to 1.8 MHz. Most converters switch at <450 kHz or >2 MHz as a result.

Even though measurement setups are slightly different, a comparison of CISPR 25 conducted limits to IT equipment conducted emissions limits defined in CISPR 32 (formerly 22) is shown in Figure 7. The most stringent limits for each standard are displayed (Class 5 for CISPR 25 and Class B for CISPR 32). One difference between the standards is that CISPR 32 conducted limits only go up to 30 MHz as compared with the 108 MHz of CISPR 25. Another difference is that CISPR 32 has defined limits across the entire frequency range (i.e., there are no "gaps") whereas CISPR 25 does have gaps. A third key difference is that CISPR 25 limits are considerably lower in magnitude than CISPR 32 limits (more than 20 dB lower at some frequencies). This is one of the reasons why some perceive the automotive emissions limits defined by CISPR 25 to be more challenging to meet than the EMI limits defined for other pieces of equipment.

IV. Emissions Mitigation Techniques

This section introduces several techniques that can be used to mitigate electromagnetic emissions from power converters. The techniques range from passive EMI filters and circuit design to modes of operation and circuit board layout tips. These techniques are broadly applicable but to focus the discussion, equipment typically powered from a 12 V lead acid battery is studied.

An overview diagram in Figure 8 shows components usually found in the power delivery path of automotive electronic control units (ECUs). The power flow is DC and goes from the input on the left (from a 12 V car battery or alternator typically) to the power converters and loads on the right. The equipment may have multiple converters connected to the input supply bus. Only a buck converter topology is shown in the diagram but there could also be boost converters, buck-boost converters, etc. The conducted noise emissions are AC in nature and propagate from the power converters on the right to the power input on the left. To be clear, the conducted noise propagates in the opposite direction of power flow.

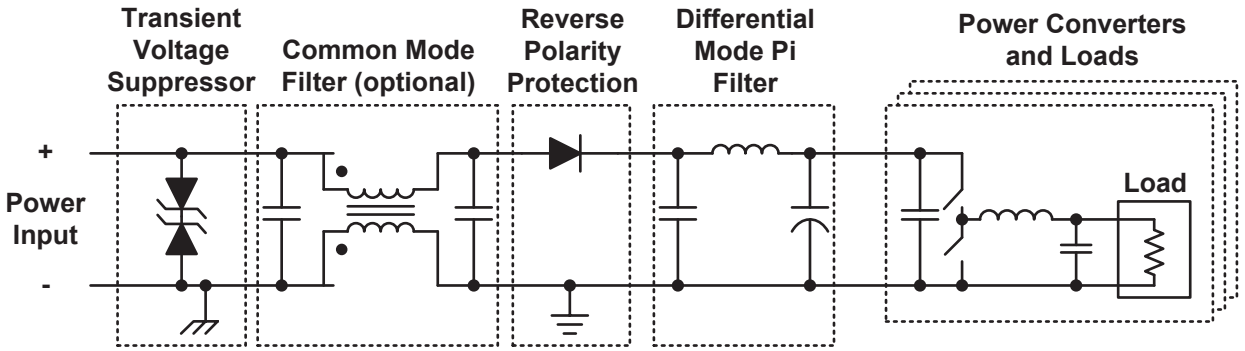

Figure 8 – Overview diagram of power delivery components in ECUs.

Two elements are used primarily for protection. A transient voltage suppressor (TVS) is included to limit the voltage seen by components downstream in the event the input voltage flies high for a period of time. The reverse polarity protection is needed in case the user accidentally connects the battery with the wrong polarity. The reverse polarity protection could use a simple diode in low-current applications but may be implemented with a MOSFET that is actively turned on when high current levels exist.

Two other elements are often included for reducing EMI. The differential-mode filter is usually included in systems with switching power converters. The common-mode filter may or may not be included depending on the application needs.

A. Differential-Mode and Common-Mode Noise

Next, it is important to understand the difference between differential-mode (DM) noise and common-mode (CM) noise. Differential-mode noise, depicted in Figure 9(a), is caused by current that flows out one input wire (+) and returns through the other input wire (-). Conversely, as shown in Figure 9(b), common-mode noise is caused by current that flows out in the same direction on both the positive and negative wires and returns through the chassis ground or a ground plane via stray capacitance.

Differential-mode noise is primarily due to the pulses of current drawn from the source by the switching power converters. This current is drawn on the positive wire and returns back on the negative wire. It creates the voltage ripple measured at a power converter's input capacitors. Differential-mode conducted emissions generally increase with load current. A pi (π) filter is used to attenuate differential-mode noise and is designed based on full load conditions. Common-mode noise, on the other hand, is mostly independent of load current. It is primarily caused by parasitic capacitances being charged and discharged each switching cycle. A common-mode choke may be used to filter common-mode noise [4].

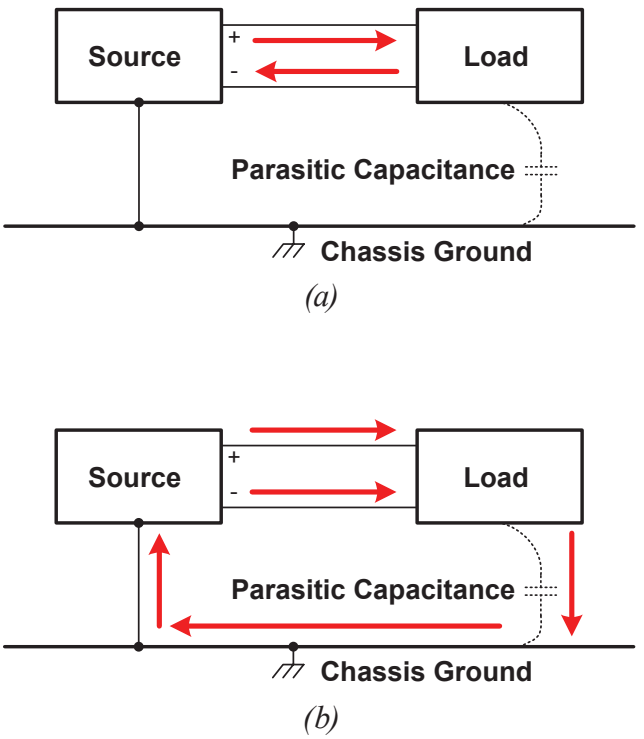

Figure 9 – Diagrams demonstrating the current flow for (a) differential-mode noise and (b) common-mode noise.

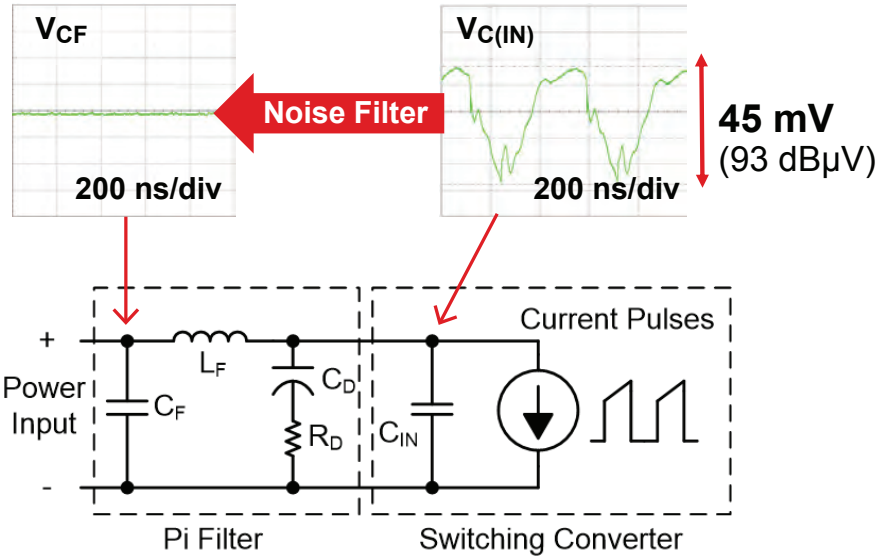

Figure 10 – A pi filter attenuates differential-mode noise by reducing input voltage ripple.

B. Differential-Mode Filter

Consider the pi filter used to reduce differential-mode noise in Figure 10. In this example, a switching converter (utilizing a buck topology perhaps) is pulling pulses of current from the input capacitor (C_{IN}) every switching cycle. The magnitude of the current pulses increases with load current, and the pulse duration depends on the duty ratio of the converter. The input capacitor voltage (V_{CIN}) has considerable ripple (in this case 45 mV or 93 dBµV) caused by the switching converter current pulses. Hence, the fundamental ripple frequency is the switching frequency. Inductor L_F and capacitor C_F form a low-pass filter that attenuates the C_{IN} voltage ripple. The voltage across C_F (V_{CF}) has considerably lower voltage ripple as desired. Capacitor C_D and resistor R_D are included for stability purposes [5-7]. Those components reduce the EMI filter output impedance peak and eliminate oscillations of the power converter input voltage.

When designing a pi filter, select L_F and C_F to get the desired attenuation at the switching frequency (f_s) as depicted in Figure 11. Assuming ideal components, choose an inductance value for L_F and then calculate the required capacitance, C_F. These two values set the resonant frequency (f_c) of the L_C filter as shown in Equation (2).

$$f_c = \frac{1}{2\pi\sqrt{L_F C_F}} \qquad (2)$$

The gain of the filter has an approximately -40 dB per decade downward slope after the resonant frequency. Set the resonant frequency to get the desired attenuation at f_s. A more detailed design procedure can be found in [8-9].

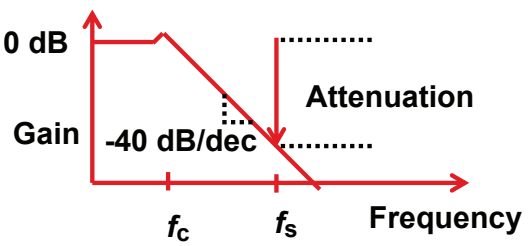

Figure 11 – Select pi filter component values to obtain the attenuation needed at the switching frequency (f_s).

The preceding discussion makes a major assumption: the filter components are ideal. In reality, the filter will have many non-ideal parasitic elements [10]. Figure 12 highlights many of the parasitic elements. The filter capacitor, C_F, will have some amount of equivalent series resistance (ESR) and equivalent series inductance (ESL). The filter inductor, L_F, will have equivalent parallel capacitance (EPC), equivalent parallel resistance (EPR) and DC resistance (DCR). The EPC results from the intrawinding capacitance of the turns of wire in the inductor.

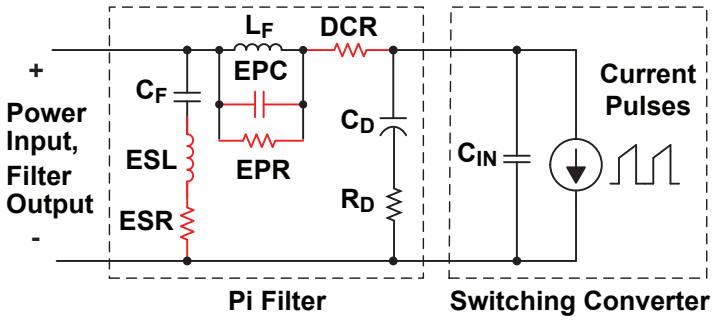

Figure 12 – Parasitic elements (shown in red) impact pi filter performance.

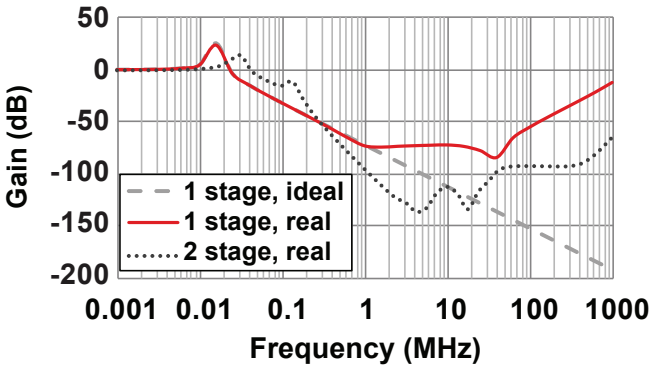

Figure 13 – Gain comparison of 1- and 2-stage pi filters with ideal components or real parasitic elements.

The parasitic elements substantially affect filter performance, especially at higher frequencies. Additional zeros and poles appear in the filter transfer function. For example, consider the filter gain comparison in Figure 13. An ideal single-stage pi filter will have a continuous -40 dB/decade downward slope after the resonant frequency. For a real one-stage filter with parasitic elements included in the model, the gain flattens out around 1 MHz and starts to increase above 40 MHz. This degrades high-frequency performance. Two-stage pi filters, as shown in Figure 14, are sometimes used to improve filter attenuation capabilities. The first-stage inductor may be a conventional inductor designed to attenuate low frequency ripple, and the second-stage filter inductor may be a ferrite bead designed to attenuate high frequency noise.

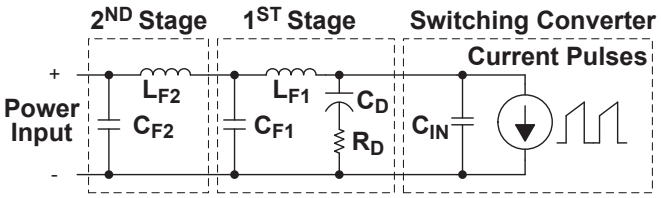

Figure 14 – Two stage pi filter.

Differential-mode noise can be modeled and simulated using many circuit simulation tools, as depicted in Figure 15. The power converter(s) can be modeled as pulsed current sources. Converter

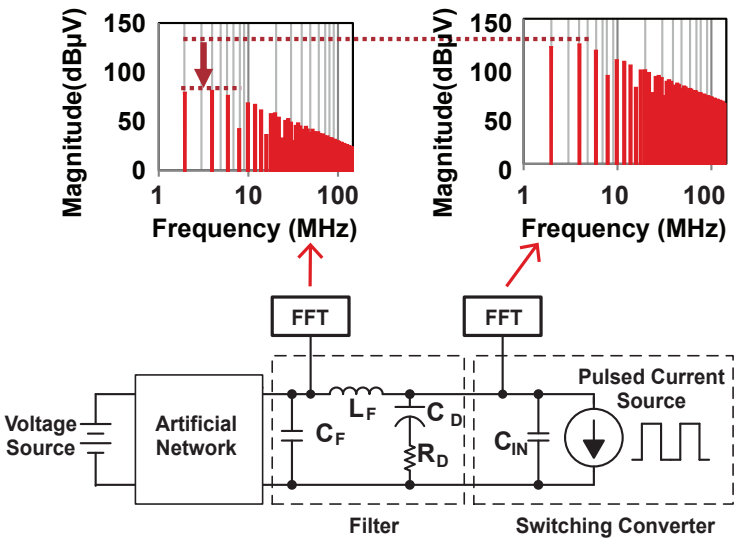

Figure 15 – Simulation framework for differential mode noise filtering.

topologies with input inductors (e.g., boost, SEPIC) would be modeled as triangular current sources with the appropriate DC value. Multiple pulsed current sources can be connected in parallel to examine the effects of phase interleaving, spread spectrum, etc. on differential-mode noise. The fast Fourier transform (FFT) block in the circuit simulator calculates the magnitude of the spectral content and can be used to estimate pi filter attenuation performance.

It is important to carefully apply simulation. Higher order parasitic elements are difficult to model accurately and are PCB layout dependent. Simulation accuracy at higher frequencies is limited. TI's WEBENCH® online simulator has an input filter design tool that estimates filter performance [11].

C. Common-Mode Noise Mitigation

Common-mode noise is often a bit more challenging to manage than differential-mode noise. The primary source of common-mode noise is parasitic capacitive coupling. It is difficult to quantify the capacitive coupling through unintended paths. Even small parasitic capacitors can couple high-frequency noise that is challenging to eliminate.

Consider the diagrams in Figure 16. The switch-node voltage (V_{SW}) ramps up and down in voltage very quickly every switching cycle. The switch node is parasitically coupled to the chassis ground or reference ground plane. This parasitic capacitance is charged and discharged as the switch-node voltage rises and falls. The parasitic capacitor current (I_{PAR}) returns through the ground plane and wiring harness. This is measured as common-mode noise. The height (h) that separates the EUT from the ground plane impacts the capacitive coupling. This is one reason that CISPR 25 defines the standard testing height to be 5 cm above the ground plane.

One of the best ways to mitigate common-mode noise is to avoid it in the first place. The overarching goal is minimizing capacitive coupling. Recall that the equation for a capacitor is

$$C = \frac{\varepsilon A}{d} \tag{3}$$

where C is capacitance, A is the area of the capacitor plates, d is the distance between the plates and ε is the dielectric permittivity. This equation suggests that to reduce capacitance we want to reduce the plate area (A) and increase the distance between plates (d). In a power converter,

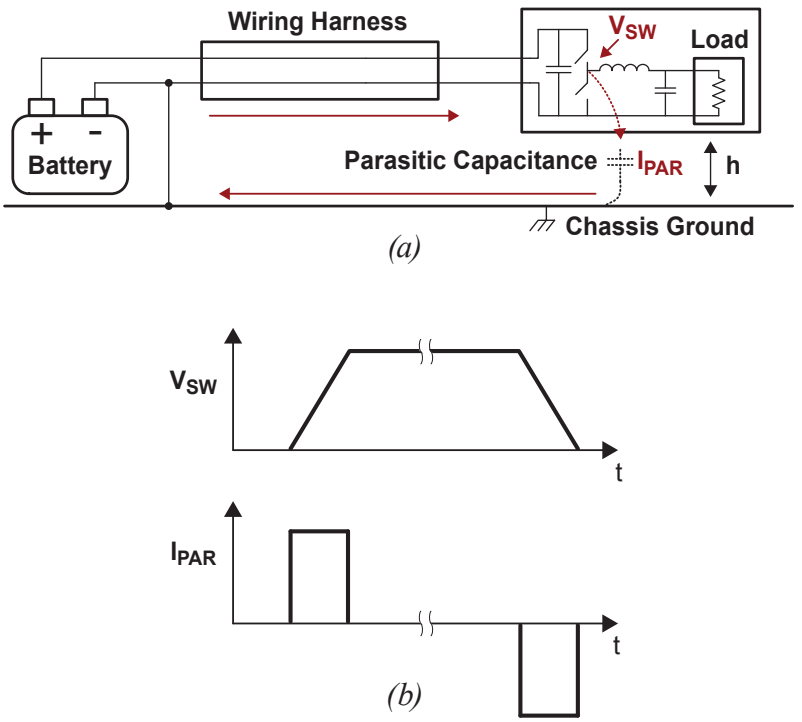

Figure 16 – Parasitic capacitive coupling from the switch node causes common-mode noise.

this translates into reducing switching node area and increasing the distance between switching nodes and sensitive circuits. Many magnetic manufacturers indicate the start terminal lead of inductors. Connect this side to the switch node to reduce switch node area. Avoid placing switching elements (e.g., inductor) on the bottom side of a circuit board to reduce capacitive coupling. Instead, keep the switching components on the PCB top side and use a ground plane to help shield switching nodes. Do not place switching nodes (main switch node, bootstrap components, snubber circuit components, etc.) near the EMI filter.

Figure 17 shows a poor layout example where the switching nodes were placed right next to the EMI filter components. This capacitively couples noise from the switching nodes to the reverse polarity protection FET. The noise bypasses the filtering in this example. When laying out EMI filters, it is common to have a cutout in the ground planes. This reduces the likelihood of noise being capacitively coupled around the EMI filter. This is especially important for common-mode chokes, which are designed to reduce common-mode noise.

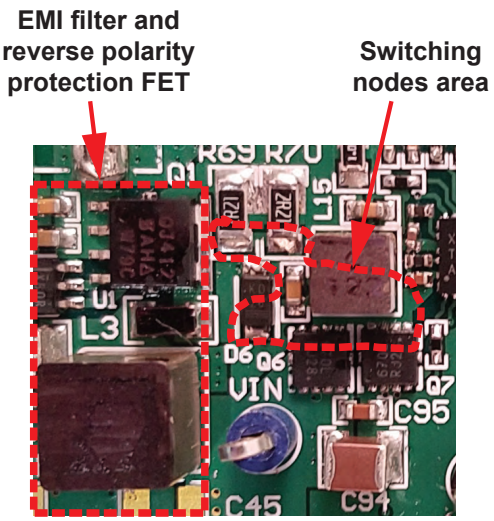

Figure 17 – A poor layout example with significant capacitive coupling due to switching nodes placed next to sensitive circuitry.

D. Reducing Magnetic Coupling

Magnetic coupling is another path for noise propagation. Avoid making antennas that propagate noise by reducing parasitic inductance. One key way to do this is to minimize the loop area of circuits carrying high di/dt currents. As shown in Figure 18, this means placing the input capacitance (C_{IN}) for a buck converter and the output capacitance (C_{OUT}) for a boost converter as close to the switching elements as possible. This should be a top priority for converter layout because it reduces the parasitic loop inductance. Have an uncut ground plane directly below the top layer. Eddy currents in the ground plane create opposing fields reducing parasitic inductance.

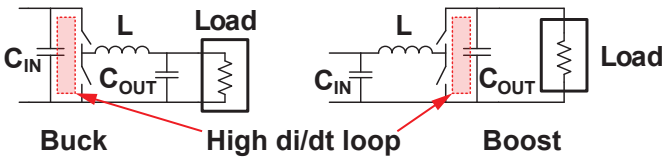

Figure 18 – Minimize high di/dt loop areas by correct capacitor placement.

Many converters have symmetrical pinouts designed to cancel magnetic fields. The input voltage (V_{IN}) and ground connections appear on two opposing sides of the integrated circuit (IC). An example is shown in Figure 19. This layout is further aided by locating small, low ESL (equivalent series inductance) capacitors as close to the IC as possible.

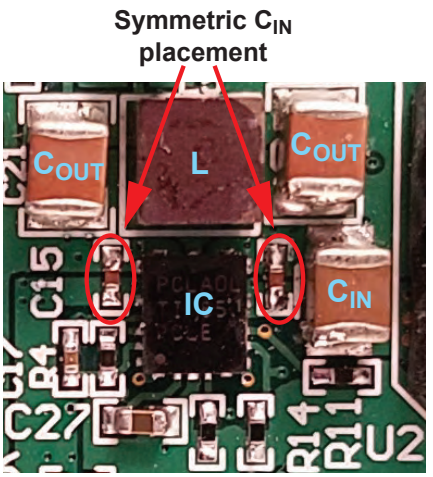

Figure 19 – Symmetric C_{IN} placement and low ESL capacitors help reduce magnetic field.

Lastly, use magnetic components (inductors and transformers) with closed magnetic paths. They are typically advertised as “shielded” components. This can cut down on stray magnetic coupling.

E. Slow Down Switch-Node Transitions

Slowing down switch-node voltage transitions can substantially improve EMI performance. This can be especially helpful in reducing high-frequency noise. Consider a trapezoidal signal, such as the switch-node voltage (V_{SW}), and its frequency content depicted in Figure 20. An envelope can be drawn around the signal spectrum with two noteworthy points. At frequency f_1, which is inversely proportional to on-time, t_{on}, the envelope of the signal spectrum decreases with a slope of -20 dB/decade. At frequency f_2, which is inversely related to the rise and fall times, t_r and t_f, the envelope of the signal spectrum begins to decrease with a slope of -40 dB/decade. The on-time is dictated by the voltage conversion ratio, but the rise and fall times can be adjusted to reduce high-frequency content. When the rise and fall times are increased, frequency f_2 decreases and the high frequency noise is reduced.

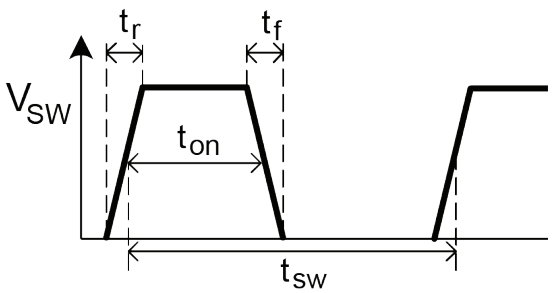

(a)

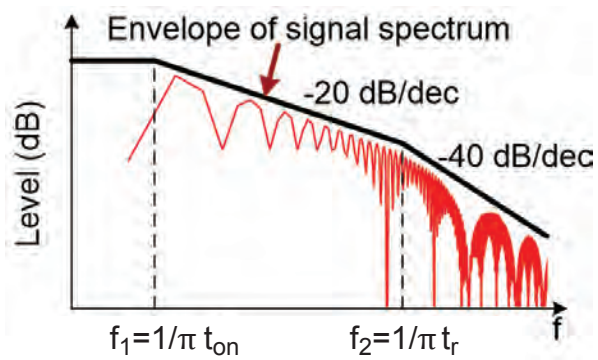

(b)

Figure 20 – The (a) trapezoidal representation of switch-node voltage and (b) its frequency spectrum.

One common technique to slow down switch-node transitions is to insert a resistor in the gate drive path. A couple of implementations are shown in Figure 21. The gate resistor, shown in Figure 21(a), slows down the turn-on/off time of the FET. Care must be taken to ensure that the FET is not inadvertently turned on and damaged when the drain voltage increases in this configuration [12]. Unintended turn-on can happen when parasitic capacitance from the gate to drain pulls up on the gate voltage, especially if the gate resistance is too large. Figure 21(b) shows another approach typically used with high-side FETs where a resistor is added in series with the bootstrap capacitor. The bootstrap resistor slows down turn-on without interfering with turn-off capabilities of the driver circuit. Although these techniques increase rise/fall times and reduce switch-node voltage ringing, they come at the expense of increased switching losses.

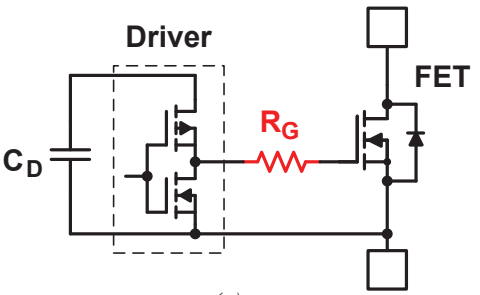

(a)

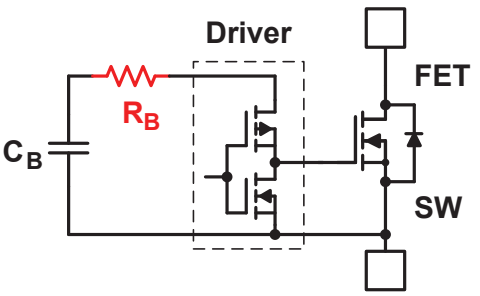

(b)

Figure 21 – Switch-node transitions can be slowed down with (a) a gate resistor or (b) a boot resistor.

F. Snubber Circuits

Snubber circuits are another technique used to reduce EMI. Snubbers shape the switch-node waveform and reduce voltage ringing. Figure 22 highlights an example snubber circuit using a resistor and a capacitor. Figure 23 shows a comparison of the switch-node voltage waveform of a buck converter with and without a snubber circuit. Without a snubber circuit installed, there is considerable ringing in the switch node voltage after the high-side switch turns on as shown in Figure 23(a). The oscillation frequency, which is between 100 MHz and 200 MHz, can show up in the emissions frequency spectrum. With a snubber circuit included, this ringing is almost eliminated. Furthermore, the peak switch-node voltage observed is reduced by over 2 V.

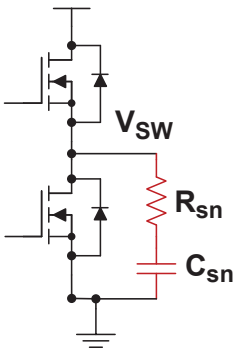

Figure 22 – A resistor-capacitor (RC) snubber circuit connected to the switch node (V_{SW}).

(a)

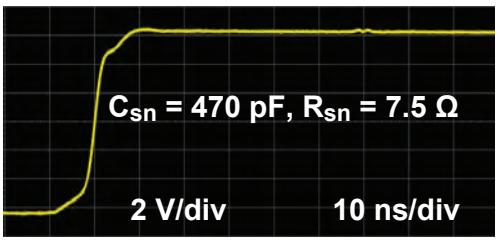

(b)

Figure 23 – A switch-node (V_{SW}) waveform (a) without a snubber and (b) with a snubber.

There are some aspects to keep in mind when using snubber circuits. There is additional power loss associated with them. This is typically estimated with Equation (4)

$$P_{loss} = C_{sn} V^2 f_{sw} \tag{4}$$

where C_{sn} is the snubber capacitance, V is the half-bridge voltage (input voltage for a buck converter or output voltage for a boost converter) and f_{sw} is the switching frequency. This power loss impacts overall converter efficiency and generates heat in the snubber resistor. There is some flexibility in component value selection but typically the snubber capacitance is chosen such that $C_{sn} > 3C_p$, where C_p is the parasitic capacitance on the switch node. A starting point for snubber resistance selection is

$$R_{sn} = \sqrt{\frac{L_p}{C_p}} \tag{5}$$

where L_p is the parasitic loop inductance and C_p is the switch-node parasitic capacitance. More detailed snubber design guidelines can be found in [13].

G. Frequency Dithering (Spread Spectrum)

Modulating the converter switching frequency can spread out the emitted noise over a wider frequency range. This technique is commonly called spread spectrum or frequency dithering and is shown graphically in Figure 24. The switching frequency is varied at a relatively slow rate (e.g., >100 times lower frequency or around the resolution bandwidth of the measuring receiver which is 9 kHz for 150 kHz to 30 MHz tests). The switching frequency is adjusted within a range of $+/-\Delta f_m$, which may be 3 to 10% of the nominal switching frequency. Several modulation schemes are possible with triangular and pseudo-random techniques being the most common [14].

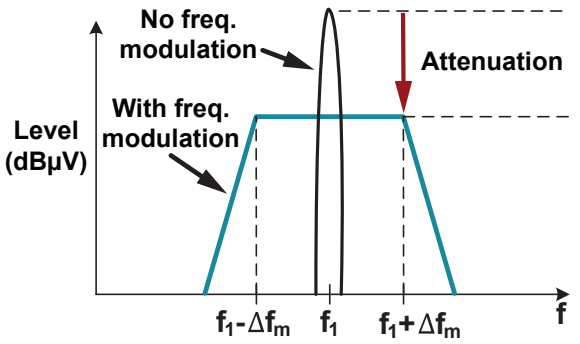

Figure 24 – Switching frequency modulation can attenuate emissions by spreading the spectrum out over a wider frequency range.

While spread spectrum is a popular technique to reduce noise emissions, it does have drawbacks. Some view it as more of a cover-up technique that does not address the fundamental noise source. It also increases the overall noise floor and is not used in certain applications (e.g., some audio and radio systems). If the modulating frequency is in the audible noise range (20 Hz to 20 kHz), this technique could generate audible noise. Another potential downside is shown in Figure 25. The frequency modulation continuously perturbs the converter and additional output voltage ripple may be observed. In the example shown in Figure 25, the output voltage ripple increases to 1.2% of the output voltage. Lastly, frequency dithering is mostly useful in reducing low-frequency content that is within the first 10 or 20 harmonics of the fundamental switching frequency. Periodic spread spectrum profiles typically do not improve high-frequency noise performance, but some pseudo-random modulation schemes may help at high frequency.

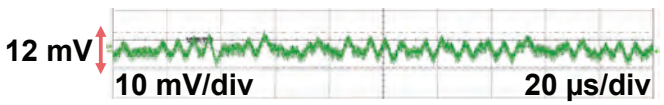

Figure 25 – Output voltage ripple on a 1 V DC supply rail with spread spectrum enabled.

H. Shield Enclosures

Metal shield enclosures can be used to contain emissions. They function like a Faraday cage and can substantially reduce radiated EMI. Grounding of the metal enclosure should be accounted for in the circuit board layout. The obvious downside is that metal enclosures add size, cost and weight in many situations.

V. CISPR 25 Test Setups

This section provides a brief overview of the CISPR 25 test setups for conducted and radiated emissions testing. CISPR 25 defines parameters like location of the equipment under test (EUT), interfacing equipment requirements and the test procedure. Further details can be found in [2-3] and the standard document itself [1].

A. Conducted Emissions Test Setup

An overview diagram for a conducted emissions test setup is shown in Figure 26. The test setup is typically housed in a shielded enclosure. A power supply (which often is a car battery) provides power to the equipment under test (EUT) through two artificial networks (AN). One artificial network is for the plus (+) terminal and one is for the minus (-) terminal. The artificial networks are similar to the line impedance stabilization network (LISN) used in other conducted EMI test setups except some of the component values are different (e.g., the inductor in the AN is 5 µH as compared to the 50 µH used in other LISNs). The AN presents a defined impedance to the EUT and represents the wiring harness in a vehicle (to a certain extent). The AN also provides a port for measuring conducted noise. The AN measurement port is connected to an EMI test receiver input. The AN port not being measured is terminated with 50 Ω. The ANs and EUT are located on a table with a metal ground plane on top. CISPR 25 defines the distance from the AN to the EUT to be 20 to 40 cm and the distance from the EUT to the ground plane to be 5 cm.

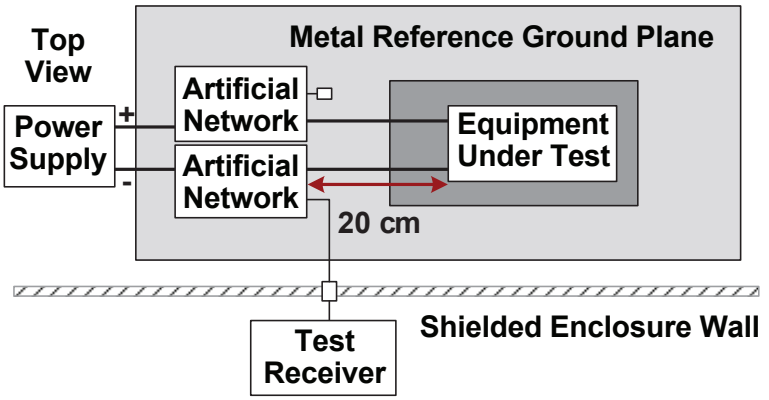

(a)

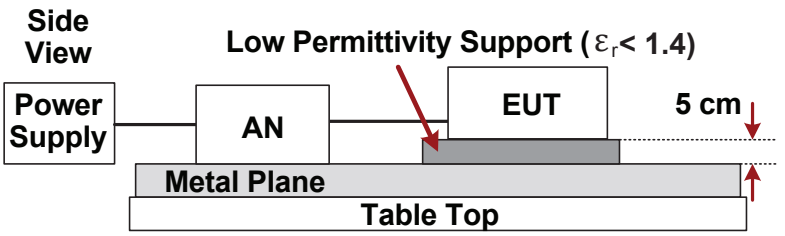

(b)

Figure 26 – CISPR 25 conducted emissions test setup from (a) top view and (b) side view.

An example conducted emissions setup is shown in Figure 27. The copper top table is in a shielded room, and the metal top is tied to the back wall to ground it. A battery is used to supply power and is connected to the artificial networks. The EUT is a little over 20 cm away from the ANs and rests on a low permittivity support that is 5 cm tall. Load resistors are connected to the EUT such that the device is operating at full load power. The conducted emissions measurement port is connected to the EMI test receiver located outside the shielded room.

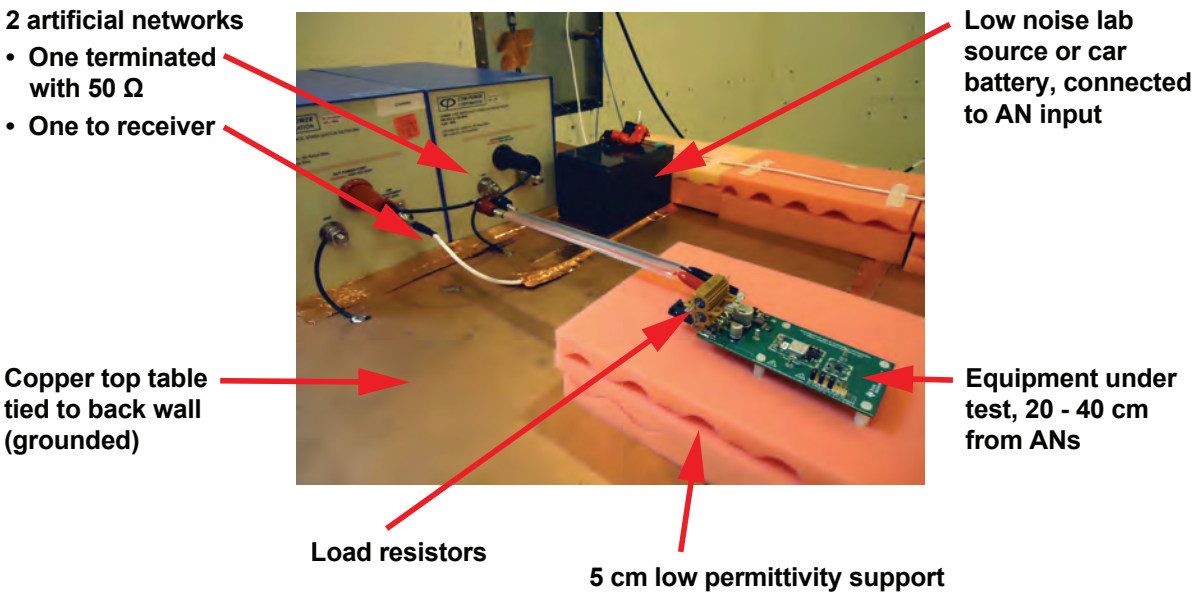

Figure 27 – Example CISPR 25 conducted emissions test setup.

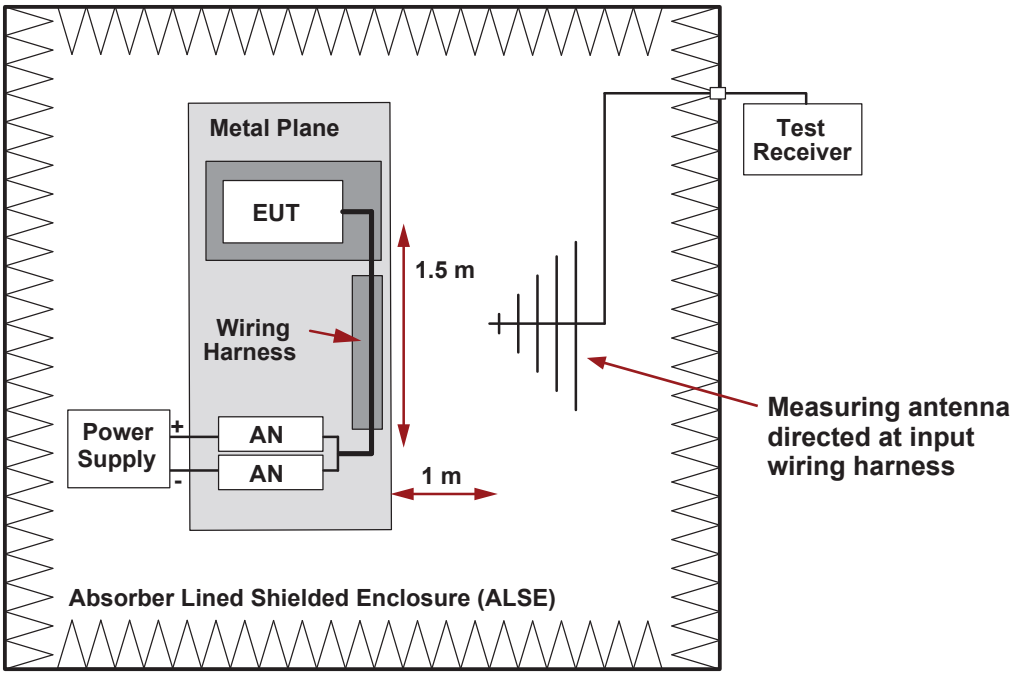

Figure 28 – CISPR 25 radiated emissions test setup.

B. Radiated Emissions Test Setup

Figure 28 shows a radiated emissions test setup according to CISPR 25. Radiated emissions are tested in an absorber lined shielded enclosure (ALSE). It is a semi-anechoic chamber with absorbing material lining the walls and ceiling but not the floor. The absorbing material reduces reflections of radiated emissions inside the chamber. There is a power supply (often a car battery) connected to the EUT through two ANs much like the conducted emissions test setup. One key difference in the radiated emissions setup is that the wiring harness connecting the ANs to the EUT is 1.5 m in length and runs parallel to the edge of the grounded metal tabletop. The measurement antenna is located 1 m away and pointed at the wiring harness (for most frequency ranges measured). This is one reason why it is best to evaluate and address conducted emissions before moving to radiated emissions. Conducted emissions that appear on the EUT wiring harness will impact radiated emissions test results.

Several images of a radiated EMI test setup are shown in Figure 29. Several antennas are used to measure across the frequency range of interest. A monopole antenna, shown in Figure 29(a), measures radiated emissions from 150 kHz to 30 MHz. A biconical antenna, shown in Figure 29(b), measures emissions from 30 MHz to 300 MHz. A log-periodic antenna, shown in Figure 29(c), typically covers the 200 MHz to 1 GHz range. A horn or log-periodic antenna may also be used to measure from 1 GHz to 2.5 GHz. The antennas are set up in both vertical and horizontal polarizations for measurements above 30 MHz.

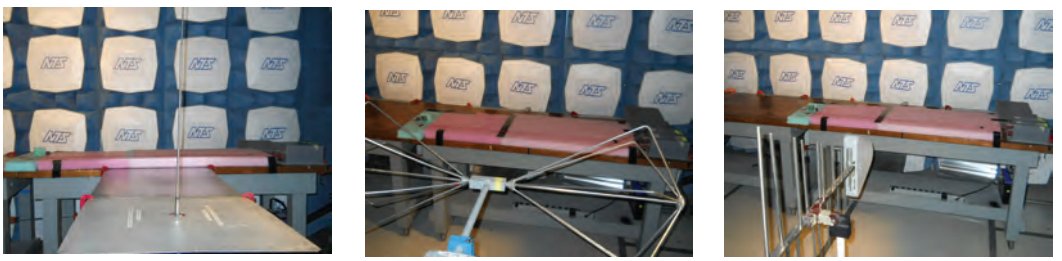

(a) *(b)* *(c)*

Figure 29 – Radiated emissions test setup with (a) monopole antenna, (b) biconical antenna and (c) log-periodic antenna.

C. Additional Test Setup Considerations

One important aspect of a test setup is the noise floor. CISPR 25 requires that the noise floor is at least 6 dB lower than the limit level. A low noise floor is required to get accurate results. First, ensure that the power supply for the setup is not injecting noise into the setup. A battery is often used to ensure a low-noise power source. The challenge with a battery is that it must be recharged between tests, and it is recommended to include proper fusing and safety mechanisms. Second, ensure that external sources of noise are eliminated. For example, a shielded room helps to reduce noise pollution from FM radio stations as shown in Figure 30.

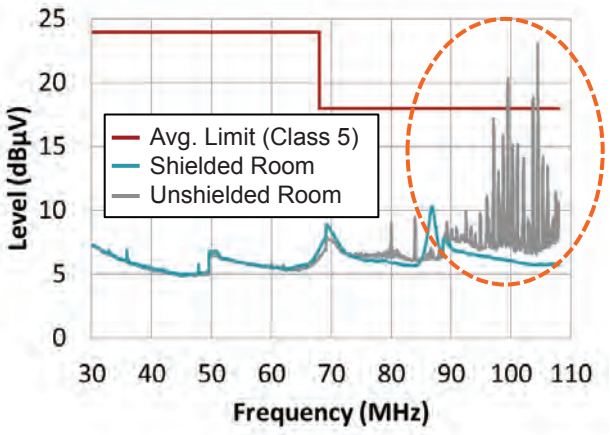

Figure 30 – Shielded rooms reduce noise from FM radio stations.

Performing EMI tests can be time consuming. It is helpful to understand EMI test receiver capabilities that can speed up testing. Classical scanning receivers and sweeping spectrum analyzers are slow because they step through measurements sequentially, as depicted in Figure 31(a). The total time it takes to run through one measurement is equal to the product of the number of data points and the dwell time per point.

An important development in recent years is the introduction of time-domain scanning [15]. Time-domain scanning was allowed by CISPR starting in June 2010 and can significantly reduce test time. The technique is shown in a simplified form in Figure 31(b). The signal being measured is sampled in the time domain. A fast Fourier transform (FFT) is applied to the sampled signal to generate the frequency-domain waveform. For a peak scan in the 150 kHz to 30 MHz range, the stepped scan time would be over 15 minutes. The same scan using time-domain scanning is less than 150 ms.

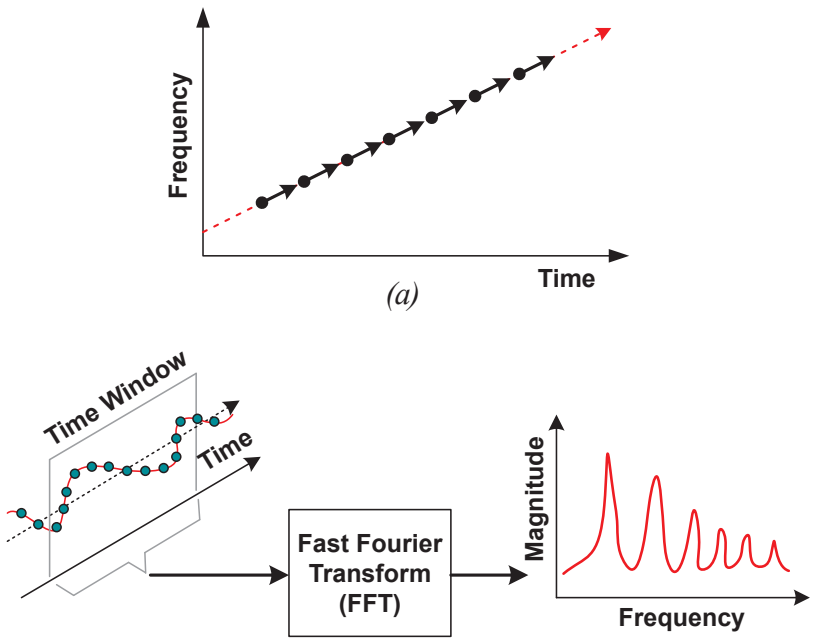

Figure 31 – EMI test receiver using (a) sequential measurements or (b) time-domain scanning.

VI. EMI Reduction Techniques Case Study

This section focuses on an experimental study of EMI reduction techniques. The aim is to provide comparative results of these mitigation techniques in an example application. The overarching goal is to show a path to get a DC/DC switching converter to pass CISPR 25 Class 5 emissions. Conducted emissions testing is selected to narrow the scope of this work.

The case study application is an off-battery converter providing a 3.3 V regulated output with up to a 5 A load current [16]. This reference design is a synchronous buck converter utilizing a synchronous buck controller with frequency spread spectrum. The design uses a dual MOSFET in power SO-8 package. The switching frequency is set to 440 kHz. While it is possible to use an integrated FET converter for this application, a controller-based design was selected due to its flexibility.

Shown in Figure 32 is a simplified schematic of the power conversion and EMI control elements of the case study. The simplified schematic shows the main power-conversion elements that affect emissions but not the controller (LM25141-Q1) and its support components. Power flows from left (battery) to right (the 3.3 V output). The topology is a synchronous buck converter with the high-side switch turned on for a portion of each switching period. The low-side FET is turned on when the high-side FET is off. The input capacitors to the left of the switches provide the current pulses through the high-side switch. The duty cycle of the high-side switch is the ratio of V_{OUT} to V_{IN}. For a 13 V typical battery voltage to a 3.3 V output, this ratio is about 0.25.

In a buck converter, the average inductor current matches the load current. When a switch is turned on, the current pulse in the switch is equal to the inductor current. The current pulses drawn by the high-side switch from the input capacitor largely determine the conducted emissions in the AM band (530 to 1800 kHz). This is why in low-current applications 2.2 MHz switching is preferred where the added switching losses do not create thermal problems. In this example with a 5 A load current, 440 kHz is chosen as the target switching frequency because it is in the 300 kHz to 530 kHz gap between the LW and AM bands. The second harmonic at 880 kHz is inside the AM band, which will be of main concern for low-frequency compliance. Harmonics in the FM band (85 to 110 MHz) present the main high-frequency challenge.

Based upon the harmonic analysis, the second harmonic content (at 880 kHz) of the main switch-node voltage waveform is 130 dBµV and of the main switch current pulses 121 dBµA. Taking the 200^{th} harmonic at 88 MHz right in middle of the FM band, values are 87 dBµV and 79 dBµA. Compare this with the Class 5 limits for average detection of 34 dBµV in the AM band and 18 dBµV in the FM band [1, 3]. Clearly, additional filtering is necessary. Based upon the ideal lumped element model, the switch-node voltage waveform will not show up on the input lines. The input current pulses are attenuated by the capacitor – inductor – capacitor of the input pi filter. However, any slight coupling of these offenders to input lines can result in failing Class 5.

This case study involves design elements that are progressively added to reduce emissions. Design elements that are studied include frequency dithering, differential and common-mode filtering on the input, snubbing the switch node and slowing of high-side gate drive turn-off. All these elements are shown in Figure 32, except for frequency dithering which comes from the controller. Slowing the high-side gate drive turn-on was not studied because it was already slowed down for FET reliability purposes. The results are intended to be descriptive for the given application; they are not intended to be prescriptive or imply the same performance in a different design.

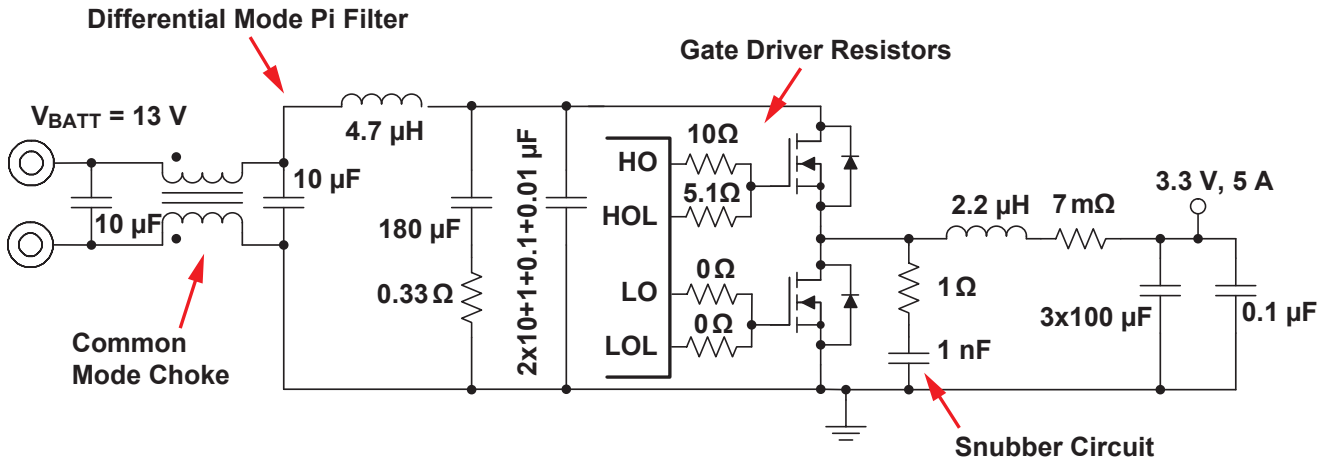

Figure 32 – Simplified schematic of case study converter with EMI mitigation components included.

A. Initial Conducted Emissions

The first step of the case study is to evaluate the initial conducted emissions spectrum without any EMI reduction techniques included. There is no input filter, no snubber circuit and no spread spectrum. The initial conducted emissions measurements are shown in Figure 33. In the AM band, the maximum peak measurement is 84.6 dBµV at 879 kHz, and the maximum average measurement at the same frequency is 84.4 dBµV. In the FM band, the max peak detect value is 46 dBµV and the max average is 41 dBµV at 92 MHz. These measurements are all failing to pass the CISPR 25 Class 5 limits by over 20 dBµV. Clearly, it is necessary to use EMI mitigation techniques in order to pass Class 5 EMI requirements.

B. Spread Spectrum (Frequency Dithering) Enabled

Next, let us examine the impact of frequency spread spectrum. Typically, this power controller feature is explored after other options have been implemented (e.g., input filtering). In this case, spread spectrum is enabled prior to other techniques because one might want to see if it is possible to pass Class 5 limits without any filtering (to save on cost and size).

The LM25141-Q1 controller has a DITH pin that allows frequency dithering to be disabled or enabled. The dithering modulation rate is set by the capacitance connected to this pin. The modulation range of the switching frequency is ±5% and the modulation method is triangular

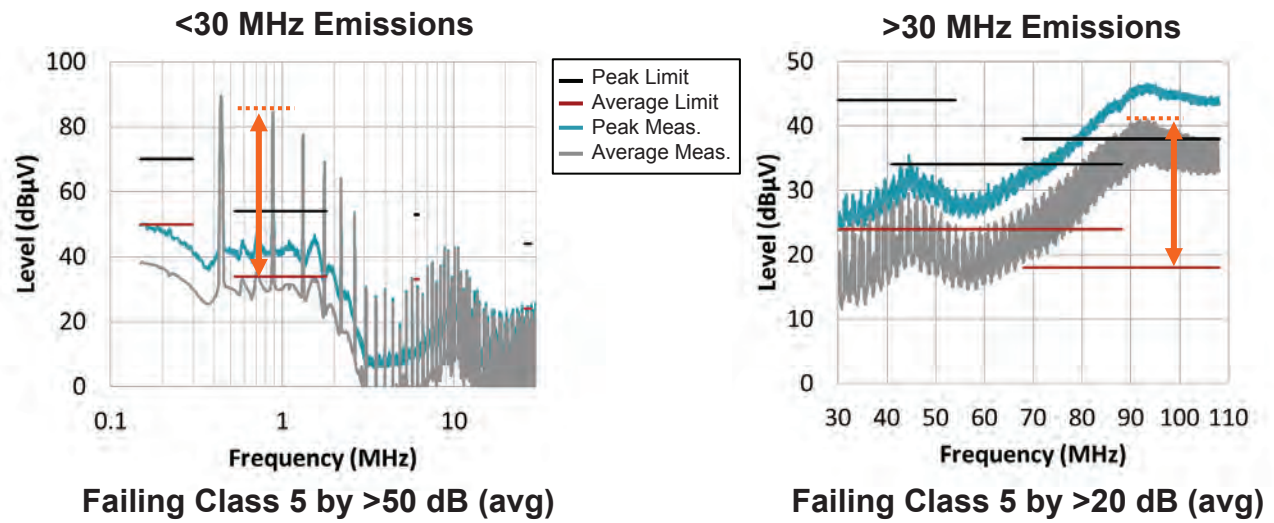

Figure 33 – Initial conducted emissions spectrum without any EMI mitigation.

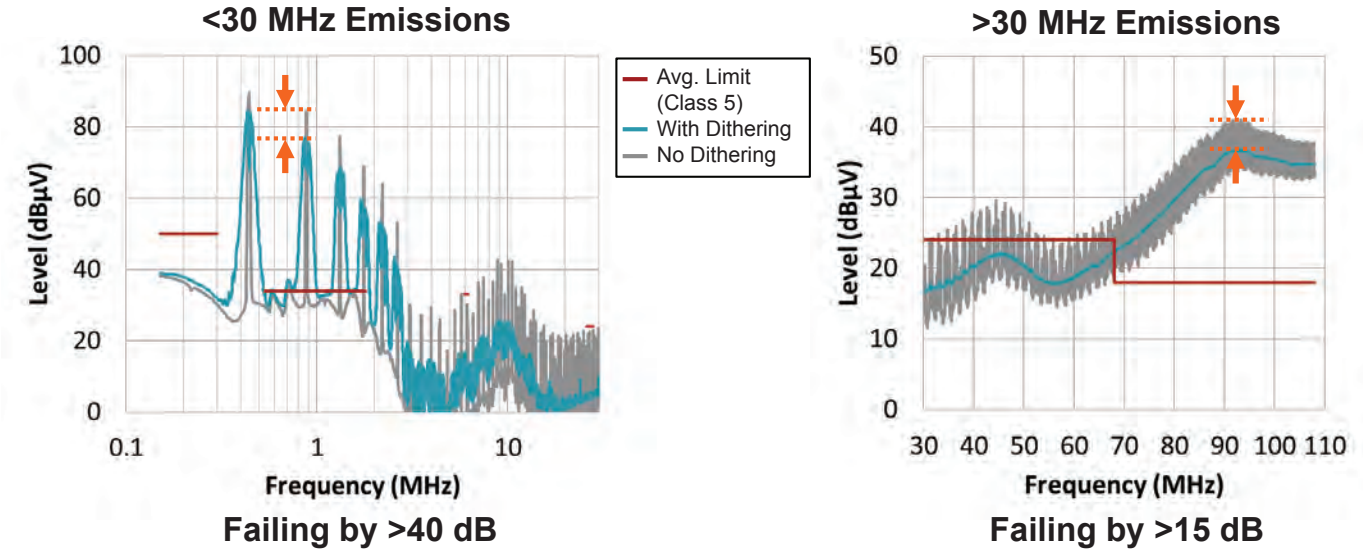

Figure 34 – Conducted emissions measurement (average detector) – dithering added.

which spreads the switching energy over the 410 to 450 kHz range. (On the test board the actual switching frequency center was shifted down 2.5% from 440 kHz to about 430 kHz due to dithering.) For harmonics of this switching frequency, the frequency band of the harmonic is the harmonic order times the width of the fundamental band. In our case, the second harmonic that is in the AM radio band is spread over an 86 kHz band centered at 860 kHz.

Figure 34 displays the measured impact of spread spectrum. The average conducted noise measured at 860 kHz with spread spectrum enabled is reduced by almost 10 dBµV compared with the results without frequency dithering. In the FM band, the worst case average drops to 37 dBµV at 92 MHz. This is 4 dBµV better than before when dithering was not turned on. Even though there are improvements with spread spectrum, an EMI filter is necessary to pass Class 5 limits.

C. Differential Mode Pi Filter Installed

The next set of results, shown in Figure 35, demonstrates the impact of a differential mode pi filter. The attenuation seen was not quite as good as the ideal calculations predicted. A 44 dBµV reduction was measured (from 76.7 dBµV at 860 kHz down to 32.5 dBµV) versus 58 dBµV per calculation. Some 860 kHz noise components from either the main switching voltage or current

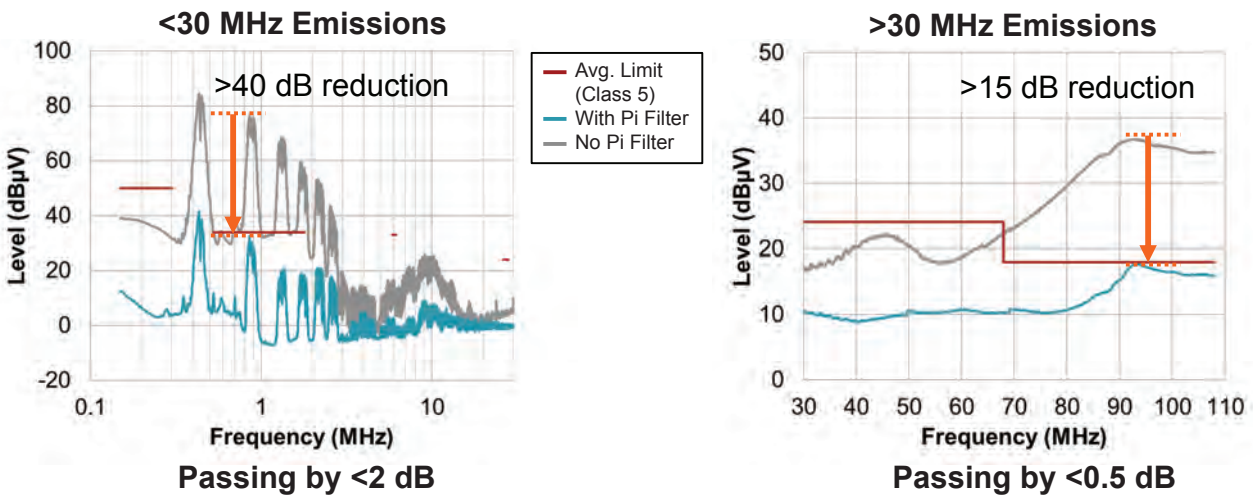

Figure 35 – Conducted emissions measurement (average detector) – differential-mode pi filter added.

bypassing the filter are probable culprits. Nonetheless, installing the differential-mode filter clearly resulted in significant reductions in the AM band, and the design passes by more than 2 dBµV in that frequency range.

The single-stage pi filter offers no common-mode filtering but still reduced the FM band noise by >15 dBµV. This shows that at least some of the FM noise is differential and not all common mode. The noise in the FB band is now below the Class 5 limits by about 0.5 dBµV. While this is technically passing, it is a very small margin. Note that frequency dithering remained enabled in this result.

D. Snubber Circuit Impact

The next technique to explore is the snubber circuit. Figure 36 shows the measured switch-node waveforms (a) without and (b) with the snubber circuit. The snubber circuit component values were R_{sn} = 1 Ω, C_{sn} = 1 nF. With the snubber circuit installed, the switch-node waveform exhibits reduced ringing, which might improve high-frequency (~100 MHz) noise results. Power loss increased a small amount (63 mW) with the snubber circuit.

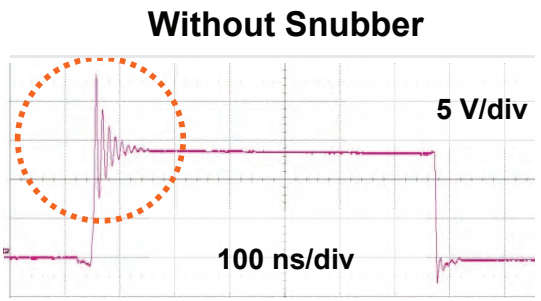

(a)

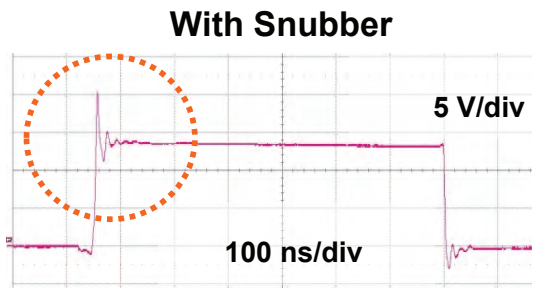

(b)

Figure 36 – Switch-node voltage waveform (a) without and (b) with the snubber circuit installed.

No significant change was seen in the conducted emissions less than 30 MHz. Somewhat surprisingly, conducted emissions actually got worse in the FM band as shown in Figure 37. A potential explanation is that while snubbers do clean up the main switching voltage waveform, they also create an additional path for rapidly changing currents and increase the high-frequency radiating loop area. An induced common-mode current harmonic in the FM band of only 1 µA will fail Class 5, even with frequency dithering. In applications where capacitive coupling dominates, such as those with an isolation transformer, snubbers may do more good than harm. Note that the differential-mode filter and spread spectrum were included in this result.

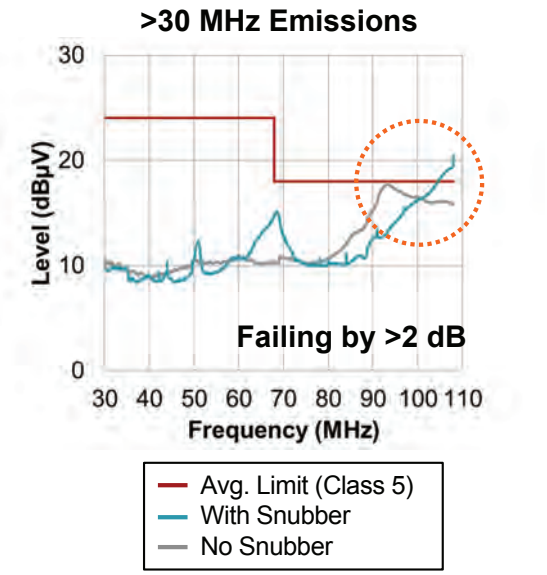

Figure 37 – Conducted emissions measurements (average detector) – snubber circuit installed.

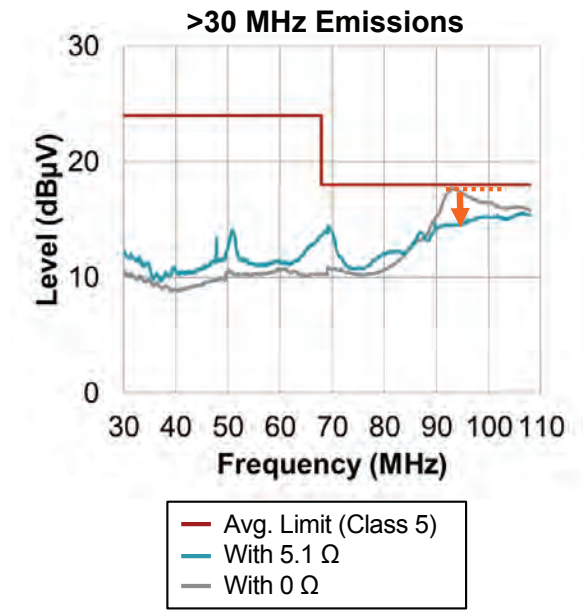

Figure 38 – Conducted emissions measurement (average detector) – gate turn-off slowed.

E. Gate Drive Turn-Off Slowed

The turn-off of the high-side switching FET was slowed by adding a 5.1 Ω resistor in the turn-off gate path. The measured conducted noise (Figure 38) shows an improvement in the FM band by about 2 dBµV for 2.5 dBµV overall margin. Added loss due to slower turn-off was ~21 mW. Further slowing did not yield an improved emissions margin. Turn-on of the same high-side FET was already slowed with 10 Ω added to the path to limit the turn-on dv/dt that could affect reliability. Adding gate resistors can be a simple, low-cost method to achieve a reduction in emissions. Note that the differential-mode filter and frequency dithering are included in this result.

F. Slip-On Ferrite Included on Input Lines

A slip-on ferrite is examined next. The results are shown in Figure 39. The best attenuation performance occurred in the FM band with 7 dBµV reduction. The lower frequency performance around 800 kHz resulted in minimal attenuation of about 1 dBµV. Note that the differential-mode filter and frequency dithering are included in this result.

G. Common-Mode Choke

The last item tested was a common-mode choke. This 4-terminal magnetic component goes on the board between the two 10 µF capacitors and provides both common-mode filtering and a second stage of differential-mode filtering due to the 1 µH leakage inductance. The results in Figure 40 demonstrate that conducted noise reduced at low and high frequencies. In the FM band, the margin was increased to 5 dBµV. At 860 kHz in the AM band, this filter resulted in more than 10 dBµV margin. Note that the differential-mode filter and frequency dithering are included in this result.

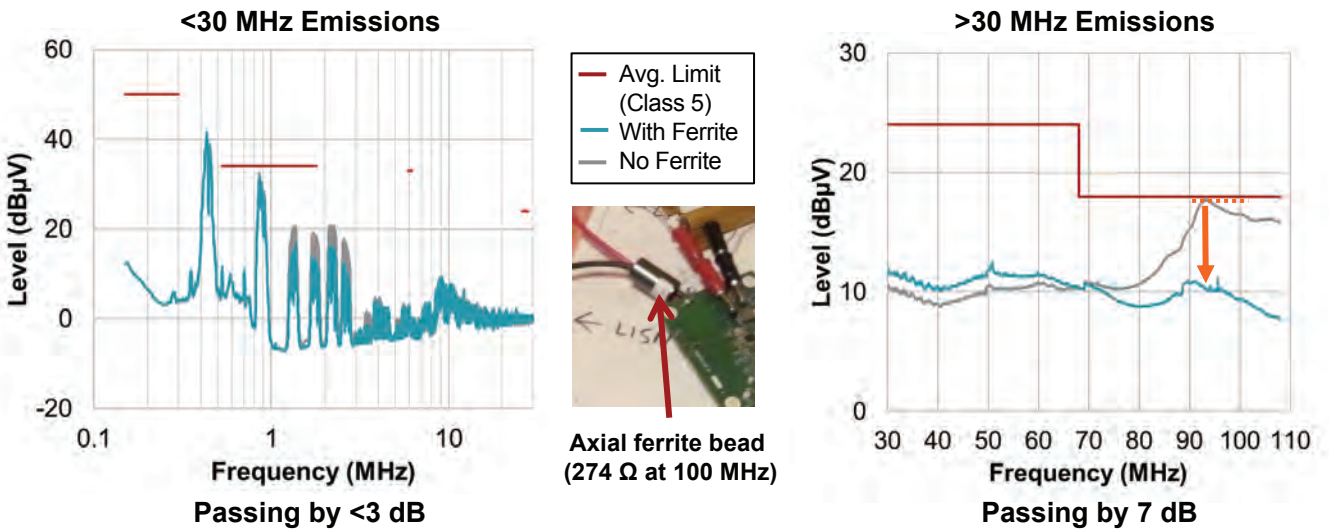

Figure 39 – Conducted emissions measurement (average detector) – external common-mode bead added.

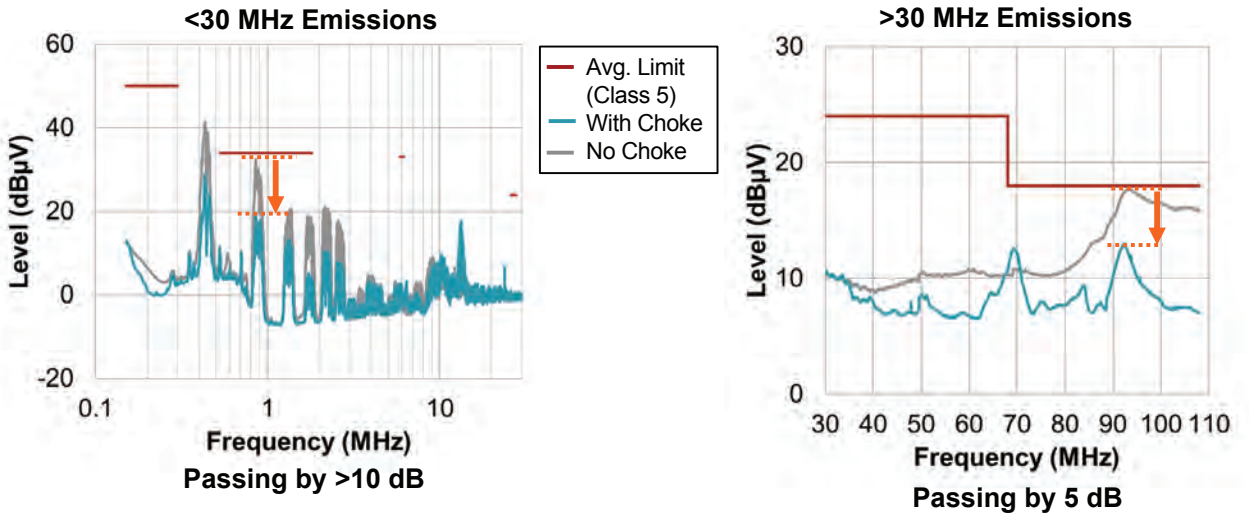

Figure 40 – Conducted emissions measurement (average detector) – common-mode choke added.

	Freq. Dithering	Differential Mode Pi Filter	Snubber	Gate Resistor	Clamp-On Ferrite	Common Mode Choke
<30 MHz reduction	5 to 10 dB	40 to 45 dB	0 dB	No impact	1 dB	>10 dB
>30 MHz reduction	5 to 10 dB	19 dB	-2 dB (got worse)	2 dB	7 dB	5 dB
Class 5	Failed by 45 dB	Passed by 0.5 dB	Failed by 2 dB	Failed by 2.5 dB	Passed by 2.5 dB	Passed by 5 dB
Additional comments		Dithering included	Dithering and pi filter included	Dithering and pi filter included	Dithering and pi filter included	Dithering and pi filter included

Table 1 – Testing summary.

H. Testing Summary

A summary of the test results is shown in Table 1. The sequence of testing was chosen to show the attenuation of the important AM and FM frequency noise components. This exercise started from the initial conducted noise levels without any EMI mitigation techniques and finally reached the low micro-volt levels needed to meet CISPR 25 Class 5. The success or failure of certain noise reduction techniques can help pinpoint whether the noise itself is due to capacitive coupling from switching waveforms or induced voltages due to high slew rate currents. In this case study the success of the common-mode choke along with the failure of the snubber to reduce noise pointed to FM band noise being due to high di/dt currents.

VII. Summary

This paper provided an overview of techniques to reduce EMI in switching power converters used in automotive applications [17-18]. CISPR 25 is a common standard used to evaluate EMC for automotive systems. The sources of EMI in switching power converters were explored along with numerous methods to mitigate emissions. These techniques range from including differential-mode and common-mode filters to slowing down switching transition rates and applying frequency dithering. Several recommendations for board layout and component selection to address the source of emissions were discussed. A case study of a 13.5 V input to 3.3 V at 5 A output converter showed the relative performance of many of these techniques. The converter was shown to pass CISPR 25 Class 5 with these EMI mitigation techniques.

References

1. IEC CISPR, CISPR 25:2016, fourth edition (or EN 55025:2017), "Vehicles, boats and internal combustion engines – Radio disturbance characteristics – Limits and methods of measurement for the protection of on-board receivers," October 27, 2016. Available: https://webstore.iec.ch/publication/26122.
2. Hegarty, Timothy, "An overview of radiated EMI specifications for power supplies," Texas Instruments White Paper SLYY142, June 2018. Available: http://www.ti.com/lit/wp/slyy142/slyy142.pdf.
3. Hegarty, Timothy, "An overview of conducted EMI specifications for power supplies," Texas Instruments White Paper SLYY136, February 2018. Available: http://www.ti.com/lit/wp/slyy136/slyy136.pdf.
4. Mamanno, Bob and Carsten, Bruce, "Understanding and Optimizing Electromagnetic Compatibility in Switchmode Power Supplies," 2002 TI Power Supply Design Seminar, 2001. Available: http://www.ti.com/lit/slup202.
5. Middlebrook, R.D., "Design Techniques for Preventing Input-Filter Oscillations in Switched-Mode Regulators," Proceedings Powercon 5, 1978.
6. Sclocchi, Michele, "Input Filter Design for Switching Power Supplies," 2011. Available: http://www.ti.com/lit/an/snva538/snva538.pdf.
7. Zhang, Charles, "Analysis and Design of Input Filter for DC-DC Circuit," November 2017. Available: http://www.ti.com/lit/an/snva801/snva801.pdf.
8. Martin, Alan, "AN-2162 Simple Success With Conducted EMI From DC-DC Converters," April 2013. Available: http://www.ti.com/lit/an/snva489c/snva489c.pdf.
9. AN-2162, Input filter calculator spreadsheet. Available: https://training.ti.com/sites/default/files/docs/InputFilterCalculator.xls.
10. Wang, S.; Lee, F.C.; Chen, D. and Odendaal, W.G., "Effects of Parasitic Parameters on EMI Filter Performance," IEEE Transactions on Power Electronics, Vol. 19, Issue 3, May 2004. Available: https://ieeexplore.ieee.org/document/1296764.
11. Texas Instruments, WEBENCH power designer. Available: http://www.ti.com/design-resources/design-tools-simulation/webench-power-designer.html.
12. Oborny, Nicholas, "Understanding Smart Gate Drive," November 2018. Available: http://www.ti.com/lit/an/slva714c/slva714c.pdf.
13. Betten, John, "Power Tips: Calculate an R-C snubber in seven steps," Power Tips Blog, May 5, 2016. Available: http://e2e.ti.com/blogs_/b/powerhouse/archive/2016/05/05/calculate-an-r-c-snubber-in-seven-steps.
14. Rice, John; Gerhke, Dirk and Segal, Mike, "Understanding Noise-Spreading Techniques and their Effects in Switch-Mode Power Applications," 2008/9 TI Power Supply Design Seminar, 2008. Available: http://www.ti.com/lit/slup269.
15. Keller, Matthias, "Comparison of Time Domain Scans and Stepped Frequency Scans in EMI Test Receivers," Rohde & Schwarz White Paper, December 2013. Available: https://scdn.rohde-schwarz.com/ur/pws/dl_downloads/dl_application/application_notes/1ee24/1EE24_1e_ESR_Time_Domain_Scan.pdf.
16. Texas Instruments, "Wide input synchronous buck converter reference design with frequency spread spectrum," January 15, 2019. Available: http://www.ti.com/tool/PMP21107.
17. Hegarty, Tim; Loke, Robert and Pace, David, "Understanding EMI and Mitigating Noise in DC/DC Converters," TI Training Video, May 11, 2017. Available: https://training.ti.com/understanding-emi-and-mitigating-noise-dcdc-converters.
18. Hegarty, T., "The engineer's guide to EMI in DC-DC converters," How2Power article series, 2017-2018. Available: http://www.how2power.com/other/EMI_Guide.php.

TI Worldwide Technical Support

TI Support

Thank you for your business. Find the answer to your support need or get in touch with our support center at

www.ti.com/support

China: http://www.ti.com.cn/guidedsupport/cn/docs/supporthome.tsp

Japan: http://www.tij.co.jp/guidedsupport/jp/docs/supporthome.tsp

Technical support forums

Search through millions of technical questions and answers at TI's E2E™ Community (engineer-to-engineer) at

e2e.ti.com

China: http://www.deyisupport.com/

Japan: http://e2e.ti.com/group/jp/

TI Training

From technology fundamentals to advanced implementation, we offer on-demand and live training to help bring your next-generation designs to life. Get started now at

training.ti.com

China: http://www.ti.com.cn/general/cn/docs/gencontent.tsp?contentId=71968

Japan: https://training.ti.com/jp

IMPORTANT NOTICE AND DISCLAIMER

TI PROVIDES TECHNICAL AND RELIABILITY DATA (INCLUDING DATASHEETS), DESIGN RESOURCES (INCLUDING REFERENCE DESIGNS), APPLICATION OR OTHER DESIGN ADVICE, WEB TOOLS, SAFETY INFORMATION, AND OTHER RESOURCES “AS IS” AND WITH ALL FAULTS, AND DISCLAIMS ALL WARRANTIES, EXPRESS AND IMPLIED, INCLUDING WITHOUT LIMITATION ANY IMPLIED WARRANTIES OF MERCHANTABILITY, FITNESS FOR A PARTICULAR PURPOSE OR NON-INFRINGEMENT OF THIRD PARTY INTELLECTUAL PROPERTY RIGHTS.

These resources are intended for skilled developers designing with TI products. You are solely responsible for (1) selecting the appropriate TI products for your application, (2) designing, validating and testing your application, and (3) ensuring your application meets applicable standards, and any other safety, security, or other requirements. These resources are subject to change without notice. TI grants you permission to use these resources only for development of an application that uses the TI products described in the resource. Other reproduction and display of these resources is prohibited. No license is granted to any other TI intellectual property right or to any third party intellectual property right. TI disclaims responsibility for, and you will fully indemnify TI and its representatives against, any claims, damages, costs, losses, and liabilities arising out of your use of these resources.

TI’s products are provided subject to TI’s Terms of Sale (www.ti.com/legal/termsofsale.html) or other applicable terms available either on ti.com or provided in conjunction with such TI products. TI’s provision of these resources does not expand or otherwise alter TI’s applicable warranties or warranty disclaimers for TI products.

Mailing Address: Texas Instruments, Post Office Box 655303, Dallas, Texas 75265